REVISION OF THE ASME SECTION III, DIVISION 3 CODE FOR PUNCTURE ANALYSIS

Douglas J. Ammerman
Sandia National Laboratories*
Albuquerque, New Mexico, 87185-0718, USA 505/845-8158

Robert E. Nickell
Applied Science & Technology
Poway, California, 92064, USA 858/485-9024

ABSTRACT

The current version of the ASME Boiler and Pressure Vessel Section III, Division 3 Code calls for design to resist puncture of lead shielded casks by use of Nelm's equation. This approach does not provide any guidance to the designer for other types of casks or for design of the inner shell in a multi-shell design. A recent ASME Code Case (N-626) provides guidance for design of the containment boundary based upon inelastic analysis.

Sandia has performed a series of tests and analyses to examine the puncture event to determine the margin of safety for any proposed new design methods. This paper will examine the results of the Sandia test and analysis series, report on ongoing activities with respect to the puncture event within the ASME NUPACK committee, and propose a broadly applicable design methodology to be included in the Code.

The purpose for changing the Code is so it provides a robust methodology for design of all cask types to resist the puncture event while maintaining current factors of safety. In general, the Code is specifically applicable to the containment boundary of these casks. However, for casks with multiple layers in their wall, the outer layer may also be important to safety, and cask designers should be able to look to the Code for guidance. Therefore, it is important to have design acceptance criteria that can be used for both the inner and outer shells of this type of cask. The work at Sandia has demonstrated that finite element analysis tools are capable of accurately predicting the response of packages to puncture events. The analyses have also shown that prediction of ductile tearing is most accurate when based on an accumulation of ductile damage failure criterion. Current ASME Code philosophy is more aligned with a stress-based acceptance criterion. This paper will discuss the validity and utility of using a stress-based acceptance criterion for design to resist puncture.

INTRODUCTION

The construction rules of the ASME Code Section III Division 3 [1] require that containment boundary elements of spent nuclear fuel and high-level waste transport packagings provide adequate protection to the public health and safety following design-basis events, such as hypothetical transport accidents. These hypothetical design-basis events include, but are not limited to, the test

---

* Sandia is a multiprogram laboratory operated by Sandia Corporation, a Lockheed Martin Company, for the United States Department of Energy under Contract DE-AC04-94-AL85000.

conditions specified in § 71.73 of Title 10 Part 71 of the Code of Federal Regulations (10 CFR 71) [2]. The puncture event involves a target puncture pin that is 6 inches (15 cm) in diameter, at least 8 inches (20 cm) long, with the edge of the pin at the initial contact surface rounded to no more than a radius of 0.25 inches (6 mm). The relatively sharp edge of the puncture pin is intended to emphasize shearing action at the pin periphery. The accident events have a low probability of occurrence, have high loading severity, and have the potential for permanent distortion and damage that could lead to complete loss of investment in the packaging. Therefore, these events are analogous to the Service Level D Conditions of the ASME Code Section III Division 1, Subsection NB [3]. Allowable stress and deformation limits for Service Level D Conditions are provided in the non-mandatory Appendix F [4].

DESIGN BY RULE VERSUS DESIGN BY ANALYSIS (CODE CASE N-626)

At present, unlike the design-by-analysis requirements for Service Level D loads in Section III Division 1, Subsection NB, the demonstration of resistance to puncture for spent nuclear fuel and high-level waste transport packaging containment boundaries is based on design by rule. This means that empirical evidence and interpreted experimental results, rather than — for example — finite element analysis methods, are used for the demonstration. In this case, experimental puncture data measured by Nelms [5] was used to generate the empirical formula:

$$\bar{E} = \frac{E}{\sigma_u t^3} = 2.35\left(\frac{d}{t}\right)^{1.6} \quad \text{which can also be expressed as:} \quad t_{req} = \left(\frac{aW}{\sigma_u}\right)^{0.71}$$

where E is the incipient puncture energy = Wh, in inch-lb, σ_u is the ultimate tensile strength of the containment boundary material, in lb/in^2, t is the containment boundary thickness, in inches, d is the diameter of the puncture pin, in inches, W is the weight of the cask, in pounds, h is the free fall height, in inches, and a is a constant that is equal to 1 for cask diameters greater than 30 inches and 1.3 for cask diameters less than 30 inches. This equation is often referred to as Nelms' equation.

Figure 1 illustrates the accuracy of Nelms' equation to puncture data available in late 1970s. The second form of it (derived setting h=40 inches and d=6 inches) was incorporated into early draft versions of Division 3, and was eventually included in the first published version of those rules. The equation can be found in WB-3324, in the design-by-rule subsection of Subsection WB.

In 1978 Larder and Arthur [6] published an extensive set of puncture test data on unbacked, lead-backed, and depleted-uranium-backed stainless steel plates. These data, which included both static and dynamic test results, showed that the Nelms' equation was very conservative. Finite element analyses by Larder and Arthur [7] showed that a better correlation could be obtained by the product of containment boundary material flow stress (e.g., 1/2 ($\sigma_u + \sigma_y$)), the containment boundary thickness, t, and the puncture pin circumference, πd, where σ_y is the containment boundary material yield strength. Figures 2 shows the correlation.

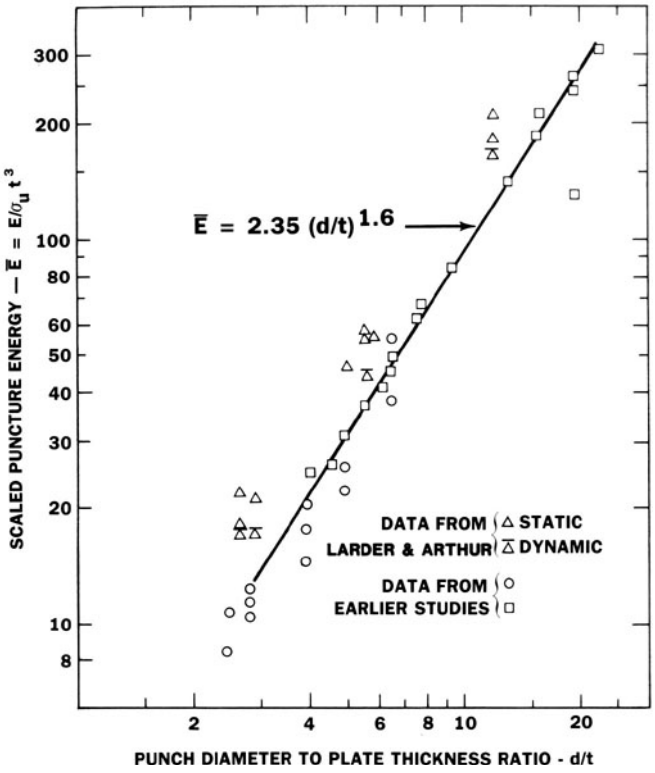

Figure 1 - Correlation of Nelms' equation with puncture data available in the late 1970s.

Later work by Nickell and May [8] on polyurethane-foam-backed stainless steel plates showed that puncture failure is determined by a combination of primary shear stress around the periphery of the puncture pin (in agreement with Larder and Arthur) and primary membrane tensile stress outside the puncture pin area. Depending upon the structural response of the backed plate system, localized deformation around the periphery of the puncture pin might dominate the failure of relatively thick plates, while more general (stretching) deformation might dominate the failure of relatively thin plates.

Reference 8 recommended the following guidance to be used in developing design-by-analysis requirements to cover potential puncture failure:

- The average shear stress in the plate around the periphery of the puncture pin and the average (membrane) tensile stress outside the periphery of the puncture pin combine to cause failure;

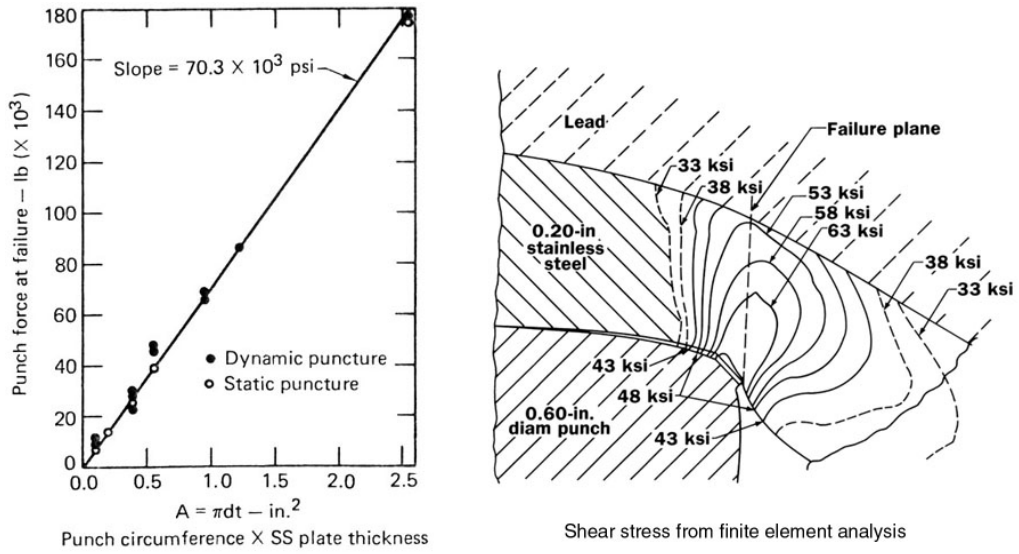

Figure 2 - Failure due to punching shear from Larder and Arthur's analysis.

- Bending stresses at the periphery of the puncture pin should be classified as secondary stresses, in analogy with the bending stresses at the edge of a flat circular head for a

cylindrical pressure vessel; these stresses cause distortion (rotation) at the puncture pin periphery, but do not cause failure unless combined with yielding (e.g., a hinge mechanism) at the puncture pin centerline;

- Bending stresses at the puncture pin centerline should be classified as primary, in order to avoid a collapse mechanism;
- The postulated puncture event should be considered a low probability event with the potential for permanent distortion, so that the design margins that apply are those contained in the non-mandatory Appendix F for Service Level D loads;
- The limits on primary stresses contained in Appendix F should be met;
- The inertial loading from the postulated puncture event is energy limited because of the prescribed drop height; and
- Membrane strain (rupture) and peak strain (ductile tearing) limits could be considered as alternatives to the Appendix F stress limits.

Much of this guidance has now been incorporated into the Division 3 Nuclear Code Case N-626, which has been approved and published [9].

REMAINING TECHNICAL ISSUES

During the deliberations on the proposed N-626 Code Case, one additional technical issue had to be resolved. Most of the existing puncture test data for the backed stainless steel plates was obtained under conditions such that shear transfer between the target plates (representing the containment boundary) and the supporting backing plates (representing gamma shielding) could be neglected. In other words, bending resistance during the puncture event was found to be provided by the target plates alone, with no significant additional bending resistance developed through shear transfer (and a subsequent increase in the moment of inertia) into the backing plates. At issue was whether significant shear coupling with the backing plates would alter the guidance provided in Reference 9, and therefore the subsequent application of the Appendix F limits to the evaluation of the puncture event.

In order to resolve this technical issue, two elastic-plastic finite element analyses were carried out for shear-coupled target and backing structure by Ammerman and Breivik [10] at Sandia National Laboratories. One of the analyses was based on a finite element model of a relatively thin target plate that was coupled in shear to a thick backing plate. This model will be refereed to as the thin shell model. The shell thickness of the thin shell model was chosen so there would not be incipient puncture, but close enough to it to test design margins. The other analysis was based on a finite element model of a relatively thick target plate that was coupled in shear to the same thick backing plate. This model will be referred to as the thick shell model. The thickness of this model was determined using Nelms' equation.

DESCRIPTION OF PUNCTURE ANALYSES

The analysis considered a cask for the transportation of spent fuel or high-level waste that had a weight of 135 tons, an inside diameter of 71.73 inches, an inner shell of 0.98 inches, a lead layer of 5.95 inches, and an outer shell of either 1.54 inches (thin shell model) or 2.6 inches (thick shell model). Figure 3 shows the geometry and mesh used for the analysis. Only the central portion of the cask was modeled, and the remaining mass was lumped into large end masses.

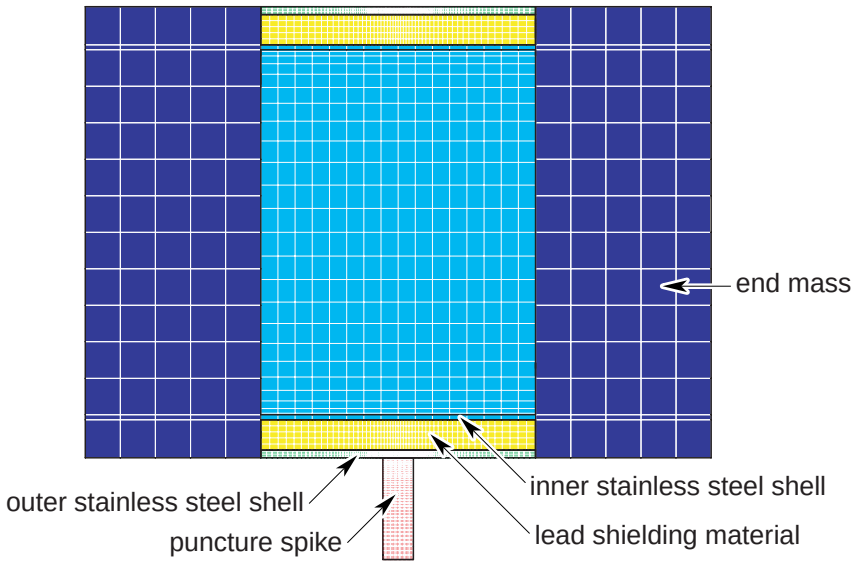

Figure 3 - Geometry of coupled shell analysis.

RESULTS

Figure 4 shows the comparison of the σ_{xx} component of the stress distribution in the outer shell. This component is the stress in the axial direction of the cask. Note that for the thick shell model (on the right in the figure) the response is typical of a bending behavior while the thin shell model shows nearly uniform membrane tension, even at the location of contact with the punch.

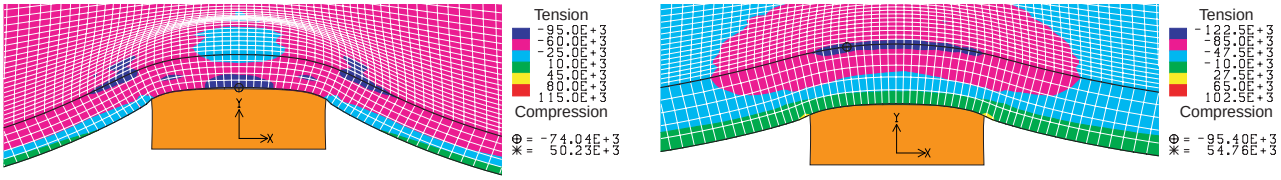

Figure 4 - Comparison of σ_{xx} for thin shell and thick shell models.

A similar behavior is seen in Figure 5 for the σ_{zz} stress, the stress in the tangential direction. Again the thin shell model has nearly uniform tension, while the thick shell model has a distribution from tension on the inner surface to compression on the surface that is contact with the punch.

The shear stresses in the xy plane are shown in Figure 6. Note that for the thin shell the maximum (indicated by ⊕ and *) occurs on the inner surface above the punch. Although it is not shown in the figure because the location is in a different plane, for the thick shell the maximum occurs on the outer surface at the location of the punch.

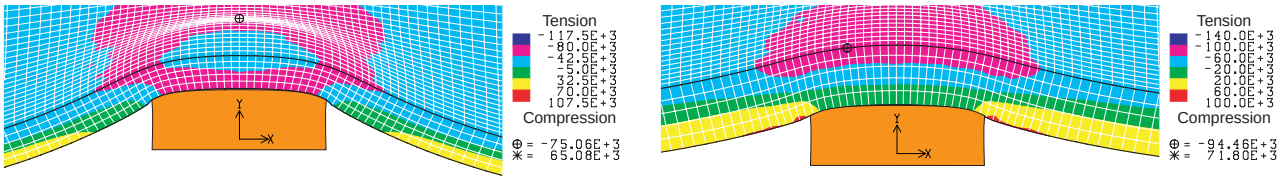

Figure 5 - Comparison of σ_{zz} for thin shell and thick shell models.

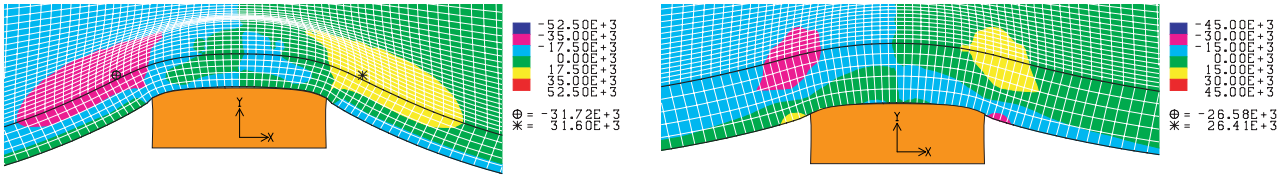

Figure 6 - Comparison of σ_{xy} for thin shell and thick shell models.

Notice that the membrane stresses in the x-direction (axial, Figure 4) and the z-direction (tangential, Figure 5) at the puncture pin periphery are very nearly equal for the thin shell model (about -50 ksi) and for the thick shell model (about -20 ksi). However, the shear stresses associated with radial bending (σ_{xy}, Figure 6) are much higher in the thin shell model analysis. Figure 6 shows a variation from about 0 ksi at the outside surface to about 32 ksi at the inside (interface) surface at the puncture pin periphery for the thin shell model and a variation from about 0 ksi on the outside surface to about 20 ksi at the inside surface for the thick shell model.

If the shear stress distribution is assumed to be parabolic in form, the "membrane" shear stress is about 21 ksi for the thin shell model and 13 ksi for the thick shell model. Assuming that σ_{yy} is sufficiently small, and that σ_{yz} and σ_{xz} are essentially zero through the target shell thickness at the periphery of the puncture pin, the principal membrane stresses can be found. In the case of the thin shell model, the principal membrane stresses at the puncture pin periphery are estimated to be (in descending order) +8.5 ksi, -50 ksi, and -53.5 ksi. For the thick shell model, the principal membrane stresses at the puncture pin periphery are estimated to be +6.6 ksi, -26.7 ksi, and -30 ksi.

Appendix F requires that, for elastic system/component analysis, the general primary membrane stress intensity be less than the smaller of 2.4 S_m and 0.7 S_u, and that the average primary shear stress across a section loaded in pure shear be less than 0.42 S_u. This general primary membrane stress intensity requirement is identical to the general primary membrane stress intensity requirement for hypothetical accident conditions given in Figure WB-3224-1. The pure shear limit is not mentioned in Figure WB-3224-1. These limits apply only when the component stresses are calculated elastically, using loads derived from an elastic system analysis (F-1331.1) or from plastic system analysis (F-1341.1). However, when the stresses are calculated using elastic-plastic stress-strain behavior, as done in this study, the general primary membrane stress intensity is limited to the greater of 0.7 S_u and $S_y + 1/3\ (S_u - S_y)$, for austenitic stainless steels. The maximum primary stress intensity at any location must not exceed 0.9 S_u. The pure shear stress limit remains the same, regardless of the method of calculation.

If S_m is taken to be 20 ksi and S_u is assumed to be 70 ksi, then 2.4 S_m controls, with a limit of 48 ksi, for elastically calculated component stresses. For shear, 0.42 S_u is 29.4 ksi. For stresses calculated with elastic-plastic material behavior, 0.7 S_u controls, with a limit of 49 ksi. The two limits on general primary membrane stress intensity are almost identical, irrespective of the method of calculating stresses.

For the Thin Shell Model, the maximum general primary membrane stress intensity is (8.5 + 53.5) = 62 ksi, which fails the Appendix F limit by a considerable margin. However, assuming pure shear loading satisfies the Appendix F limit, but with about 30% margin. This illustrates the fact that the rules of Appendix F are conservative, since the Thin Shell Model appears to have some additional

resistance to puncture, based on the shear stress and the remaining margin against formation of a plastic hinge at the puncture pin centerline.

For the Thick Shell Model, the maximum general primary membrane stress intensity is (6.6 + 30) = 36.6 ksi, which satisfies the Appendix F general primary membrane stress limits, with about 30% margin. Assuming pure shear loading satisfies the Appendix F limit, with over 100% margin. The Thick Shell Model is in no danger of forming a plastic hinge at the puncture pin centerline.

MARGIN OF SAFETY

The stresses shown from the above analyses indicate in a qualitative manner that neither shell will experience ductile tearing and punch-through. Prior tests and analyses conducted at Sandia have shown that failure can be predicted by measuring the accumulation of tensile damage [11]. Figure 7 shows the comparison of this tearing parameter for the two cases. Failure by tearing occurs, for 304 stainless steel, when this parameter reaches 1.3. The Thin Shell Model has a margin of about 145% and the Thick Shell Model has a margin of about 260% against failure.

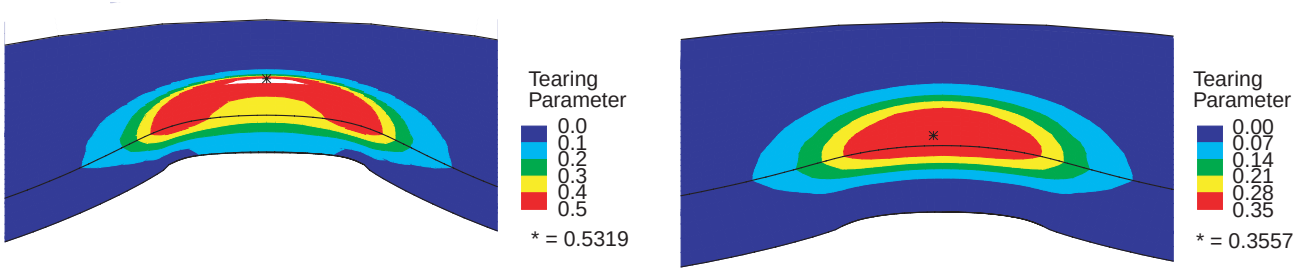

Figure 7 - Comparison of tearing parameter for thin shell and thick shell models. For 304 stainless steel, failure occurs when the tearing parameter reaches 1.3.

CONCLUSIONS

The design by analysis method encompasses a larger spectrum of conditions than the design by rule method (e.g. casks with shielding material other than lead). The thick shell model used in this paper just meets the design by rule required thickness, but has considerable margin using design by analysis. The design by analysis method still results in a considerable factor of safety relative to ductile tearing of the shell. The thin shell model used in this paper does not meet the design by analysis criteria, but has a margin against ductile tearing of more than 100%. The ASME Subgroup NUPACK has approved the design by analysis method discussed in this paper. The proposed changes are being reviewed by Section III for formal inclusion in Division 3. If approved, this will allow designers to determine the wall thickness required to prevent puncture by use of the analysis methods discussed here or by continuing to use the design by rule method currently included in WB-3324.

REFERENCES

[1] "Containment Systems and Transport Packagings for Spent Nuclear Fuel and High Level Waste," ASME Code Section III, Division 3, Subsection WB, ASME International, New York, NY, 1998 Edition.

[2] "Packaging and Transportation of Radioactive Material," Title 10, Part 71, Code of Federal Regulations, U. S. Nuclear Regulatory Commission, Washington, DC.

[3] "Rules for Construction of Nuclear Power Plant Components," ASME Code Section III, Division 1, Subsection NB – Class 1 Components, ASME International, New York, NY, 1998 Edition.

[4] "Rules for Construction of Nuclear Power Plant Components," ASME Code Section III, Division 1, Appendices, Appendix F – Rules for Evaluation of Service Loadings with Level D Service Limits, ASME International, New York, NY, 1998 Edition.

[5] Nelms, H. A., "Structural Analysis of Shipping Casks," Report No. ORNL-TM-1312, Oak Ridge National Laboratory, Oak Ridge, TN, 1968.

[6] Larder, R. A. and Arthur, D., "Puncture of Shielded Radioactive Material Shipping Containers: Part II – Static and Dynamic Tests of Laminated Plates," NUREG/CR-0930 (UCRL-52638), Lawrence Livermore National Laboratory, Livermore, CA, 1978.

[7] Larder, R. A. and Arthur, D., "Puncture of Shielded Radioactive Material Shipping Containers: Part I – Analysis and Results," NUREG/CR-0930 (UCRL-52638), Lawrence Livermore National Laboratory, Livermore, CA, 1978.

[8] Nickell, R. E. and May, R. A., "Design of Radioactive Material Shipping Packaging for Low-Velocity Puncture Resistance," Nuclear Engineering and Design, Vol. 74, No. 2, pp. 223-232, February 1982.

[9] "Use of Plastic Analysis for the Design of Type B Containment Components for Nuclear Material Transportation Casks", ASME Boiler and Pressure Vessel Code Case N-626, ASME International, New York, NY, 1999.

[10] Ammerman, D. J. and Breivik, N. L., "Use of Inelastic Analysis in Cask Design", Proceedings of the Embedded Topical Meeting on DOE Spent Nuclear Fuel and Fissile Material Management, ANS Annual Meeting, pp. 353-358, San Diego, CA, June 4-8, 2000.

[11] Breivik, N. L., Ammerman, D. J., Eifert, E. J., Ludwigsen, J. S., and Radloff, H. D., "Experimental and Analytical Determination of the Puncture Resistance of Transportation Casks", SAND2001-xxxx, Sandia National Laboratories, Albuquerque, NM, to be published.